Journal of
Composites Science

MDPI

Article

High β-Phase PVDF Copolymer Nanocomposite Films with Dielectric and Piezoelectric Behavior

Lorenzo Broggio [1,2,*], Giacomo Moretti [1], Sandra Dirè [1] and Andrea Dorigato [1,2]

[1] Department of Industrial Engineering, University of Trento, Via Sommarive 9, 38123 Trento, Italy; giacomo.moretti@unitn.it (G.M.); sandra.dire@unitn.it (S.D.); andrea.dorigato@unitn.it (A.D.)
[2] National Interuniversity Consortium of Materials Science and Technology (INSTM), Via G. Giusti 9, 50121 Florence, Italy
* Correspondence: lorenzo.broggio-1@unitn.it

Abstract

Polymer–ceramic piezoelectric composites are widely investigated to combine the high piezoelectric performance of ferroelectric ceramics with the flexibility and processability of electroactive polymers. However, achieving enhanced dielectric properties while preserving the intrinsic piezoelectric response of the polymer matrix remains challenging, particularly due to dielectric mismatch between the constituent phases and interfacial effects. In this work, barium titanate ($BaTiO_3$) loaded poly(vinylidene fluoride-trifluoroethylene) (PVDF-TrFE) nanocomposites were fabricated by solvent casting using polyvinylpyrrolidone (PVP) and polysorbate 80 (PS80) as dispersing agents, aiming to obtain polarizable materials capable of retaining high piezoelectric strain coefficient (d_{33}) values and potentially exploiting the opposite polarity of matrix and filler through tailored poling strategies. Morphological, crystallographic, structural, thermal, thermomechanical, dielectric, and piezoelectric characterizations were performed by SEM/EDXS, XRD, FTIR, DSC, TGA, DMTA, dielectric spectroscopy, and d_{33} measurements. Both dispersants improved filler dispersion and film densification, increasing the crystalline fraction of the matrix, without altering the relative fraction of β-phase (up to 93%). PVP enabled moderate and stable permittivity enhancement with weak frequency dependence, whereas PS80 introduced an electrically active interfacial contribution that amplified low-frequency permittivity at high filler loadings but made the permittivity more frequency-dependent. The piezoelectric response (between −20 pC/N and −25 pC/N) remained predominantly governed by the polymer phase, suggesting limited polarization played by $BaTiO_3$. These results underlined the critical role of interfacial electrical properties in designing stable high-performance flexible PVDF-TrFE/$BaTiO_3$ composites.

Keywords: piezoelectricity; nanocomposites; PVDF; PVDF-TrFE; $BaTiO_3$; poling; energy harvesting

Check for updates

Academic Editor: Roberto Scaffaro

Received: 25 April 2026
Revised: 19 May 2026
Accepted: 21 May 2026
Published: 23 May 2026

Copyright: © 2026 by the authors. Licensee MDPI, Basel, Switzerland. This article is an open access article distributed under the terms and conditions of the Creative Commons Attribution (CC BY) license.

1. Introduction

The increasing demand for self-powered systems in wearable electronics, Internet of Things (IoT) sensors, and biomedical implants has driven significant interest in flexible piezoelectric materials capable of harvesting energy from environmental mechanical sources such as vibrations and human motion. Piezoelectric nanogenerators convert such mechanical energy into electrical energy, offering promising solutions for autonomous

power supplies in distributed sensing systems [1]. Among piezoelectric materials, traditional piezoceramics such as lead zirconate titanate (PZT) exhibit very high electromechanical coupling and piezoelectric coefficients (d_{33} up to 600 pC/N) [2], making them highly efficient ferroelectric materials for energy conversion. However, their inherent brittleness, limited processability, and high density restrict their integration into flexible devices. Moreover, PZT contains lead (Pb), whose use is increasingly regulated due to serious environmental and health concerns associated with lead exposure [3]. For these reasons, lead-free perovskite ceramics such as barium titanate ($BaTiO_3$, BT) have emerged as environmentally friendly alternatives with good piezoelectric performance and reduced toxicity [1,3]. In contrast to ceramics, piezoelectric polymers such as poly(vinylidene fluoride) (PVDF) and its copolymer poly(vinylidene fluoride-trifluoroethylene) (PVDF-TrFE) have attracted considerable attention owing to their mechanical flexibility, low density, biocompatibility, and ease of processing into thin films or fibrous structures, making them particularly suitable for wearable and flexible devices. PVDF is known to crystallize in several polymorphic forms: five crystalline phases (α, β, γ, δ, and ε) are most commonly reported in the literature, each corresponding to distinct chain conformations and dipole arrangements [4–6]. In the α-phase, polymer chains adopt a trans-gauche-trans-gauche′ (TGTG′) conformation within a centrosymmetric monoclinic unit cell, resulting in antiparallel dipole arrangements and negligible piezoelectric activity [7,8]. The δ-phase can be viewed as a polar variant of the α structure, whereas the ε-phase is considered an antipolar analogue, although both are less commonly encountered in conventional processing [6,9]. By contrast, the orthorhombic crystal β-phase structure, with an all-trans (TTTT) planar zigzag chain conformation, facilitates alignment of the C–F dipoles in the same direction and, for this reason, it is the most polar and exhibits the strongest ferroelectric and piezoelectric responses, making it the most desirable for electroactive applications [10–12]. The γ-phase also exhibits an orthorhombic lattice and possesses a polar structure but with a mixed trans-gauche sequence (TTTGTTTG′) and can contribute to piezoelectricity, but its spontaneous polarization and piezoelectric activity are significantly lower than those of the β-phase because of the presence of gauche bonds that reduce the net dipole moment per unit cell [13]. Thus, while both β- and γ-phases are electroactive, the β-phase is preferentially targeted in piezoelectric materials design for energy harvesting and sensing applications [14,15]. Despite this, the overall piezoelectric response of PVDF remains lower than that of piezoceramics, with typical longitudinal piezoelectric coefficients (d_{33}) in the range of 10–20 pC/N for oriented films. The incorporation of trifluoroethylene (TrFE) with an extra C-F bond into the polymer backbone promotes the stabilization of the electroactive crystalline β-phase by favoring all-trans chain conformations. This modification reduces the energetic barrier for β-phase nucleation and enables the material to achieve a high degree of polar ordering without the need for mechanical stretching. Furthermore, the presence of TrFE units decreases the interactions between adjacent molecular segments and modifies the dipole–dipole coupling, leading to a reduction in the Curie temperature (T_c) relative to neat PVDF [16]. As a result, PVDF-TrFE copolymers exhibit enhanced ferroelectric properties, including higher remanent polarization and lower coercive fields, because the β-phase is more readily formed and stabilized during processing and poling [6,7,17,18]. Several strategies have been explored to further enhance the dielectric and piezoelectric performance of PVDF-based composites, including optimization of filler morphology and size, surface functionalization, interface engineering, and control of the polymer crystalline phase. Recent studies have shown that tailoring interfacial interactions and promoting β-phase stabilization can significantly improve dipolar polarization and electromechanical response in flexible ferroelectric nanocomposites [19,20]. Embedding $BaTiO_3$ particles into a PVDF-TrFE matrix to form 0–3 type composites has been investigated as a strategy to

synergistically combine the high piezoelectric activity and dielectric constant of the ceramic with the flexibility and processability of the polymer, resulting in enhanced dielectric permittivity and piezoelectric responses [1]. Studies have shown that adding BT can promote β-phase formation and improve overall piezoelectric performance [21], although the magnitude of the improvement depends on particle content, dispersion quality [22], and poling methodology [23,24]. Achieving uniform dispersion of $BaTiO_3$ nanoparticles within the polymer matrix remains a critical challenge in ferroelectric composites because inadequate dispersion or agglomeration of particles can lead to localized dielectric heterogeneities, stress concentrations, and reduced poling efficiency, ultimately compromising device performance [1,25]. SEM evidence and dielectric studies have shown that untreated $BaTiO_3$ particles tend to cluster within polymer matrices, deteriorating electrical and mechanical properties if not properly stabilized [26,27]. Particle's modification and dispersion strategies are therefore employed to enhance filler–matrix compatibility and improve microstructural uniformity [26,28,29]. One effective approach is the use of polymeric non-ionic dispersants such as polyvinylpyrrolidone (PVP). PVP can adsorb onto ceramic particle surfaces via its polar lactam groups, forming a steric barrier that reduces particle–particle attraction and promotes finer dispersion within the polymer matrix. Studies on PVP-coated $BaTiO_3$ have demonstrated improved dispersion and significantly enhanced dielectric performance in polymer composites compared to uncoated BT, as evidenced by more uniform distributions and increases in permittivity [30,31]. In contrast to ionic dispersants, which may introduce mobile charges that screen ferroelectric domains and increase dielectric losses, non-ionic surfactants, such as polysorbate 80 (PS80), operate via steric stabilization and interfacial energy minimization. These agents improve particle wettability and dispersion in organic media without contributing significantly to ionic conductivity, thereby reducing the risk of space charge formation and dielectric loss. Although specific studies on PS80's effects in piezoelectric polymer composites are less common, the broader colloidal chemistry literature supports its role in enhancing dispersion stability through its long polyoxyethylene chains and hydrophobic moieties, which interact favorably with both inorganic fillers and polymer chains [32]. Overall, polymeric dispersants like PVP and non-ionic surfactants such as polysorbate 80 represent valid non-ionic strategies for improving BT dispersion: PVP primarily provides steric barrier effects through surface adsorption, while surfactants improve interfacial wetting and particle stabilization. However, systematic comparisons of their influence on phase crystallization, interfacial polarization, and electromechanical performance in PVDF-TrFE/$BaTiO_3$ composites remain scarce in the literature. This work addresses this gap by fabricating PVDF-TrFE/BT nanocomposites using PVP and PS80 as dispersants, followed by comprehensive characterization of dispersion quality, thermal characterization, and dielectric/piezoelectric responses from flexible devices. By elucidating how dispersant type influences β-phase content and device output, the study paves the way for optimized and scalable composites for advancing autonomous powering for next-generation electronics.

2. Materials and Methods

2.1. Materials

The thermoplastic matrix selected for this study was the FC25 poly(vinylidene fluoride-co-trifluoroethylene) (PVDF-TrFE) copolymer, purchased from ARKEMA SA (Colombes, France) in the form of white powder (density = 1.77 − 1.82 g/cm^3, melting temperature = 150 °C, molecular weight = 450 kDa, (75/25 molar ratio). The filler was barium titanate ($BaTiO_3$), with an average particle diameter of 500 nm, purchased from Acros Organics BV (Geel, Belgium) in the form of ceramic powder (purity = 99%, density = 6.08 g/cm^3). Polyvinylpyrrolidone (PVP) was purchased from Sigma Aldrich

Inc. (Saint Louis, MO, USA) in form of solid powder (density = 1.2 g/cm^3 at 25 °C, molecular weight = 29 kDa), polysorbate 80 (PS80) was purchased from Sigma Aldrich Inc. (Saint Louis, MO, USA) with the commercial name of Tween 80 (TW80) in form of viscous liquid (density = 1.064 g/mL at 25 °C, molecular weight = 79 kDa). Acetone (density = 0.791 g/mL at 25 °C, purity ≥ 99.5%) and N,N-dimethylformamide (DMF, density = 0.944 g/mL at 25 °C, purity = 99.8%) were both purchased from Sigma Aldrich Inc. (Saint Louis, MO, USA).

2.2. Sample Preparation

The filler, the matrix, and the dispersant were dried in a vacuum oven overnight at 80 °C, while all other materials were used without any pretreatment. The sample preparation route is schematized in Figure 1. $BaTiO_3$ and a non-ionic dispersant (PVP or PS80, 5 wt% with respect to $BaTiO_3$) were premixed in DMF to obtain a subsequent polymer-to-solvent ratio of 1:9 w/w, and subjected to ball milling (ball to powder ratio 10:1) to promote efficient adsorption of the dispersant onto the particle surface, thereby achieving a more homogeneous and stable dispersion. The PVDF-TrFE powder was subsequently introduced into the dispersion and stirred for 30 min to obtain a homogeneous solution. After a degassing step, the resulting mixture was cast onto a biaxially oriented polypropylene (BoPP) substrate by means of a doctor blade system AB4400, supplied by TQC Italia SRL (Seregno, MB, Italy), equipped with a VF1824 applicator. Solvent removal was carried out by heating the casting plate at 55 °C for 1 h, followed by 90 °C for 2 h under a laminar air flow. The film was then transferred to a vacuum oven and annealed at 130 °C for 3 h to ensure complete solvent removal and promote β-phase crystallization and stabilization in the matrix. The final thickness of the produced samples ranged between 40 µm and 50 µm. Table 1 summarizes the developed samples and their relative composition.

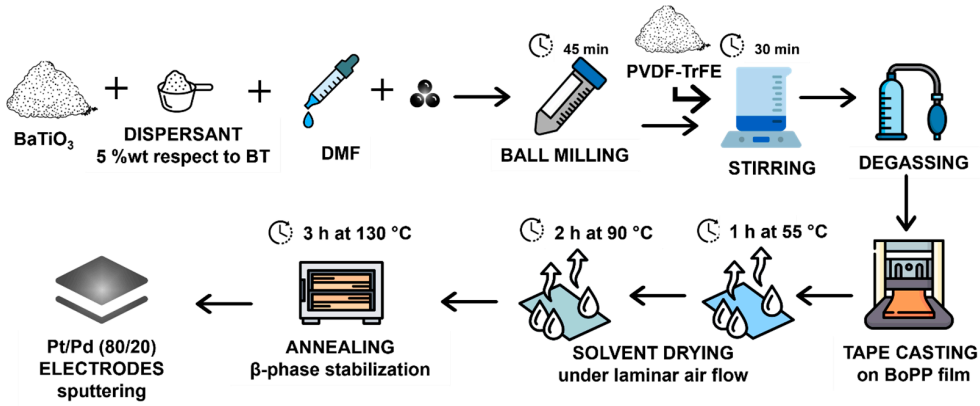

Figure 1. Film preparation route for all the produced samples.

Table 1. Relative compositions of all the produced samples.

Sample	PVDF-TrFE (vol%)	$BaTiO_3$ (vol%)	Dispersant [1]
P	100	-	-
P_5PVP	95	5	PVP
P_10PVP	90	10	PVP
P_20PVP	80	20	PVP
P_5PS80	95	5	PS80
P_10PS80	90	10	PS80
P_20PS80	80	20	PS80

[1] 5 wt% with respect to the $BaTiO_3$ wt%.

2.3. Poling Treatment

The poling treatments adopted in the present investigation are schematized in Figure 2 together with the utilized poling setup. Prior to the poling process, Pt/Pd layers of approximately 4 nm were sputtered through a mask onto the samples to act as circular electrodes (1.5 cm diameter) and ensure an effective application of the electric field. During the contact poling process, square specimens (2×2 cm^2) were positioned between a high-voltage electrode and a grounded counter-electrode. To prevent dielectric failure caused by air, the entire assembly was submerged in an FR3 natural ester insulating oil bath (Cargill Inc., Minneapolis, MN, USA). Immersion enabled the application of elevated electric fields without triggering breakdown phenomena. To perform an effective poling, it was necessary to take into account the opposite piezoelectric response that emerges from the two phases of the composite when subjected to the same electric field (i.e., negative d_{33} of PVDF-TrFE and positive d_{33} of $BaTiO_3$). A one-step poling was performed, subjecting the films to a constant positive DC electric field of +20 kV/mm at 120 °C for 15 min, then the temperature was lowered to room temperature before removing the electric field. Alternatively, a two-step poling was performed: initially, a constant positive DC electric field of +20 kV/mm was applied at 125 °C (T_c of $BaTiO_3$) for 30 min; then, a constant negative DC electric field of −20 kV/mm was applied at 100 °C (below T_c of PVDF-TrFE) for 10 min; and finally, the samples were cooled to room temperature before removing the electric field [23,24,33]. All samples were connected to a discharge setup with both sides grounded overnight. This allows the samples to be discharged so that there are no accumulated charges that could affect the piezoelectric measurements.

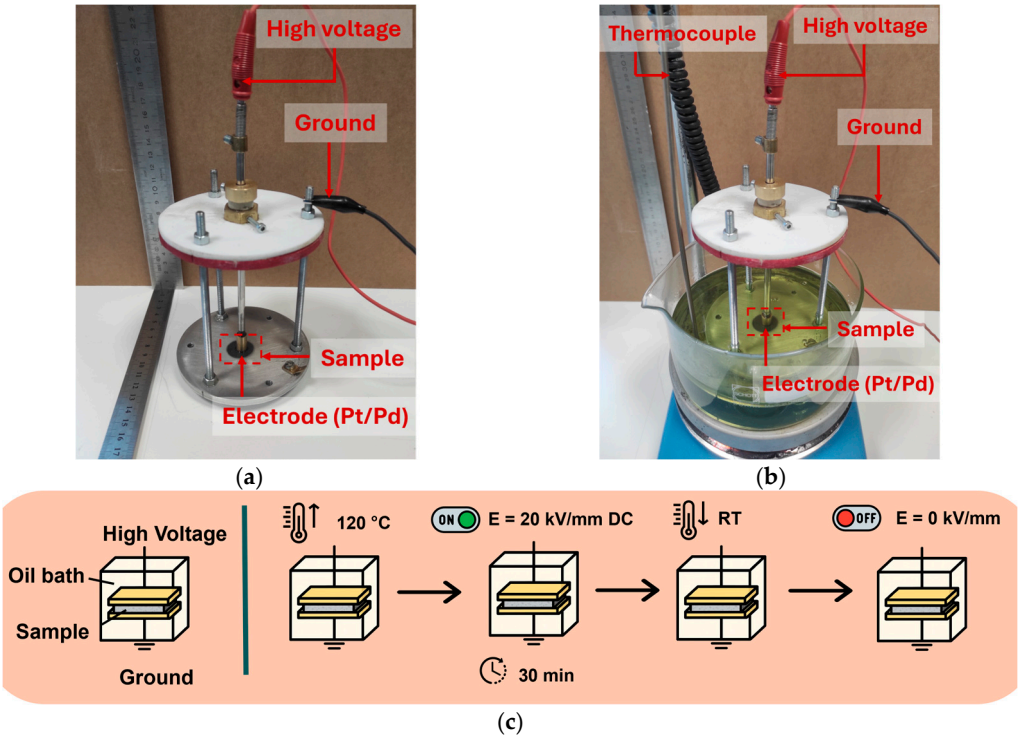

Figure 2. *Cont.*

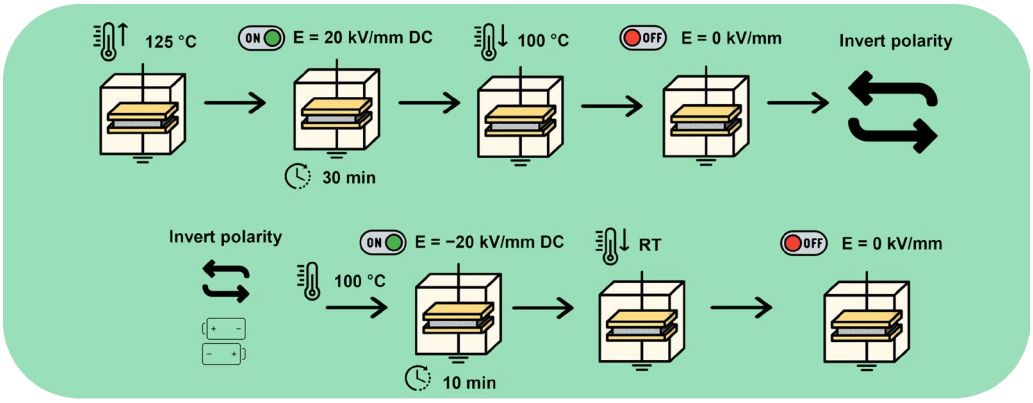

(**d**)

Figure 2. (**a**) Poling setup with high voltage and ground connections in air and (**b**) immersed in insulating oil; (**c**) one-step poling procedure and (**d**) two-step poling procedure applied on the prepared nanocomposite films.

2.4. Experimental Techniques

To investigate the elemental composition and distribution of the constituent phases within the composite, the lateral surfaces of the samples were observed by scanning electron microscopy (SEM) equipped with energy-dispersive X-ray spectroscopy (EDXS). The analyses were performed using a JEOL IT300 scanning electron microscope equipped with an EDXS detector, operating at an accelerating voltage of 20 kV. Elemental mapping was carried out to assess the distribution of the elements present in the composite and to evaluate the homogeneity of the filler within the sample cross-section. In addition, the acquired micrographs were used to determine lognormal BT size distribution curves by means of at least 200 measurements performed using the ImageJ (ver. 1.53e) software.

Field emission scanning electron microscopy (FESEM) images of the cryo-fractured surfaces of the prepared films were acquired by using a Zeiss SUPRA 40 FE-SEM (Carl Zeiss Industrielle Messtechnik GmbH, Oberkochen, Germany), operating at an accelerating voltage of 10 kV. Prior to the observations, the samples were fixed on a metallic stub through the use of a conductive strip and then underwent Pt-Pd (80:20) sputtering by means of a Q150T coater (Quorum Technologies Ltd., Lewes, UK).

X-ray diffraction (XRD) measurements were performed on an Italstructures IPD3000 diffractometer (GNR Analytical Instruments, Novara, Italy), equipped with a Cu anode source (at 40 kV, 30 mA) coupled to a parallel multilayer optics (AXO-DRESDEN GmbH, Dresden, Germany). Samples were positioned flat on a zero-background substrate and scanned in reflection geometry. XRD patterns were collected by means of a MYTHEN multichannel silicon strip detector (DECTRIS AG, Baden, Switzerland) over a 10–110° 2-theta range (0.02° step size) in continuous scan mode (30 min total acquisition time). XRD data were analyzed by means of the Rietveld methodology as implemented in the Maud software (ver. 2.99993) [34]. The crystal structure for β PVDF-TrFE and its polymorphs were modeled with Crystallographic Information files for standard PVDF as reported in Hasegawa et al. [35]. Based on preliminary diffraction data analysis, a three-phase model was adopted for quantitative phase analysis of the PVDF-TrFE/$BaTiO_3$ composites, consisting of three contributions, namely PVDF-TrFE in its crystalline β-phase, $BaTiO_3$, and an amorphous polymer fraction. This choice was motivated by the clear identification of the β crystalline form of PVDF-TrFE in all samples, together with the presence of $BaTiO_3$, while no additional crystalline polymorphs could be unambiguously detected within the resolution limits of the technique. The possible presence of other PVDF-TrFE polymorphs was therefore considered either negligible or below the detection threshold, likely due to nanocrystalline disorder or their absence in the investigated systems. The amorphous

polymer fraction was simulated using a single pseudo-Voigt peak with large full width at half maximum (FWHM), introduced to reproduce the broad diffuse shoulder of the main PVDF-TrFE reflection located at approximately 18.5° [23,36]. Quantitative phase analysis was carried out by refining the intensity scale factors and the background contribution. The background was modeled using a third-degree polynomial function in order to avoid overfitting of the diffuse scattering signal. The resulting weight fractions were subsequently renormalized, considering the known reference content of $BaTiO_3$ in the composites. In addition, the average volume-weighted crystallite size of PVDF-TrFE was refined, together with the lattice parameters of $BaTiO_3$. No additional XRD characterization was performed on the neat $BaTiO_3$ powder, as its structural analysis was reported in detail in a previous study of our research group [37].

Fourier-transform infrared (FTIR) spectroscopy was performed in attenuated total reflectance (ATR) mode by using a Perkin-Elmer Spectrum One spectrometer (Perkin-Elmer GmbH, Waltham, MA, USA) equipped with a ZnSe crystal and operating in a wavenumber range 650–4000 cm^{-1}; 50 scans were collected for each spectrum (resolution: 4 cm^{-1}). The determination of the crystalline phases of PVDF-TrFE involved the identification of their characteristic peaks as follows: α-phase can be detected at 764 cm^{-1}, 975 $cm^{-1,}$ and 1212 cm^{-1}; β-phase at 840 cm^{-1} and 1275 cm^{-1} (1275 cm^{-1} is exclusive to β-phase); γ-phase: 812, 832, 840, and 1234 cm^{-1} (1234 cm^{-1} is exclusive to γ-phase) [4,38–40]. The fraction of polar phase F(β, γ) was determined according to Equation (1) [41]:

$$F(\beta,\ \gamma) = \frac{A_{\beta,\gamma}}{\left(\frac{K_{\beta,\gamma}}{K_\alpha}\right)A_\alpha + A_{\beta,\gamma}} = \frac{A_{\beta,\gamma}}{1.26A_\alpha + A_{\beta,\gamma}} \quad (1)$$

where A_α and $A_{\beta,\gamma}$ are the absorbance at 764 cm^{-1} and at 840 cm^{-1}, respectively, while $A_\alpha = 6.1 \cdot 10^4$ cm^2/mol and $A_{\beta,\gamma} = 7.7 \cdot 10^4$ cm^2/mol are the corresponding absorbance coefficients. The α-phase fraction could be calculated as $F(\alpha) = 1 - F(\beta,\gamma)$.

Thermal characterization of the prepared films was conducted by differential scanning calorimetry (DSC) using a Mettler DSC 5+ calorimeter (Mettler Toledo Inc., Columbus, OH, USA). Specimens with a mass of approximately 10 mg were inserted in aluminum pans and analyzed following a heating–cooling–heating protocol over a temperature range from −60 °C to 170 °C, with a scanning rate of 10 °C/min for both heating and cooling steps. All measurements were performed under a continuous nitrogen purge at a flow rate of 100 mL/min. The DSC measurements allowed to determine the melting and crystallization temperatures of the polymeric phase (T_m and T_{cr}), as well as the associated enthalpy values (ΔH_m and ΔH_{cr}). The degree of crystallinity (χ) was calculated according to Equation (2), taking into account the cold crystallization contribution:

$$\chi = \frac{\Delta H_m - \Delta H_{cc}}{\Delta H_0 \cdot w} \cdot 100 \quad (2)$$

where ΔH_{cc} represents the cold crystallization enthalpy, ΔH_0 corresponds to the melting enthalpy of a fully crystalline polymer, assumed to be 104.7 J/g [42,43], w is the weight fraction of PVDF-TrFE. Finally, DSC measurements allowed to determine the Curie temperature (T_c) and the specific enthalpy value associated with this transition (ΔH_c).

Thermal stability of the material was evaluated by thermogravimetric analysis (TGA) using a Q5000 IR thermobalance (TA Instruments Inc., New Castle, DE, USA). Approximately 10 mg of material was heated from 30 °C to 700 °C at a constant rate of 10 °C min^{-1} under an inert nitrogen atmosphere with a flow rate of 10 mL/min. The TGA measurements allowed to determine the onset temperatures associated with specific mass losses of 1 wt%, 3 wt%, and 5 wt% ($T_{1\%}$, $T_{3\%}$, $T_{5\%}$), the residual mass at 700 °C ($m_{R,700}$), and the

characteristic degradation temperature (T_d), defined as the temperature corresponding to the maximum of the first derivative of the mass loss curve (DTG).

Dynamic mechanical thermal analysis (DMTA) was performed using a DMA Q800 instrument (TA Instruments Inc., New Castle, DE, USA) to investigate the material response to stress and temperature at constant frequency. Rectangular specimens (4×30 cm^2) were tested in tensile mode at a frequency of 1 Hz over a temperature range from -70 °C to 140 °C, with a heating rate of 3 °C/min. The storage modulus (E'), loss modulus (E''), and loss factor ($tan\delta$) were measured as a function of temperature. One specimen was tested for each composition.

Dielectric breakdown tests were performed to determine the maximum applicable electric field for the poling process. To achieve an efficient application of the electric field, Pt/Pd electrodes of around 4 nm thickness were sputtered onto the samples to create a set of electrodes. In particular, one face of the samples was fully coated with a ground electrode, while high-voltage circular electrodes (3 mm diameter) were coated on the other side with a mask, with a minimum distance of at least 5 mm between adjacent electrodes. A DC voltage ramp was applied to the samples in a parallel-plate electrode configuration, and the electric field was increased at a constant rate of 0.1 kV/s until electrical failure occurred. The breakdown strength (E_{BD}) was calculated as the ratio between the breakdown voltage and the sample thickness, previously measured using a micrometer. Measurements were carried out at room temperature under ambient conditions. At least five specimens were tested for each sample. The results of this analysis allowed the definition of a practical reference for safe poling conditions.

Dielectric characterization was performed using a precision LCR meter (LCX100, Rohde & Schwarz GmbH & Co. KG, Munich, Germany) operating over a frequency range from 4 Hz to 300 kHz. Measurements were conducted by applying an AC excitation voltage of 10 V while sweeping the frequency at selected values of 4 Hz, 10 Hz, 100 Hz, 1 kHz, 10 kHz, 100 kHz, and 300 kHz. The relative dielectric permittivity (ε_r) was determined from the measured capacitance (C) values by rearranging Equation (3):

$$C = \varepsilon_0 \varepsilon_r \frac{A}{d} \tag{3}$$

where ε_0 is the permittivity of free space, A represents the effective electrode area, and d is the sample thickness.

The piezoelectric response of the polarized samples was assessed through the determination of the longitudinal piezoelectric coefficient d_{33} (generally reported in pC/N or pm/V), measured using a high-precision Berlincourt piezometer (PKD3-2000, PolyK, Singapore) with alternating force of 0.25 N, and 110 Hz frequency, while static pre-load was set to 10 N. For each poling condition, at least three independent measurements were collected.

3. Results and Discussion

The results obtained from energy-dispersive X-ray spectroscopy (EDXS) on samples with PVP and PS80 dispersants are reported in Figures 3 and 4, respectively. EDXS recognized the bright little regions as BT inclusions and the darker gray parts as the polymer matrix. Despite the PVP surface mediation, regions with enriched oxide contents appear to form. However, percolation is prevented by the particles' good separation from one another. The elemental distribution obtained from EDXS mapping of barium exhibits marked differences, indicating variations in the spatial dispersion of the Ba-containing phase within the composites, with the amount of included filler. In particular, all the samples show a certain agglomeration of the filler, which is more marked and visible in the 10 vol% filled samples. Indeed, P_10PVP and P_10PS80 nanocomposites report a higher

particle mean size value and a broader lognormal size distribution curve compared to the other samples. Meanwhile, samples with 5 vol% and 20 vol% filler content display less pronounced differences in mean particle size and distribution width. The literature reports that isolated nanoparticles are observed at low filler contents, while particle aggregation and morphological irregularities emerge as the filler content increases, due to the onset of particle–particle interactions [44].

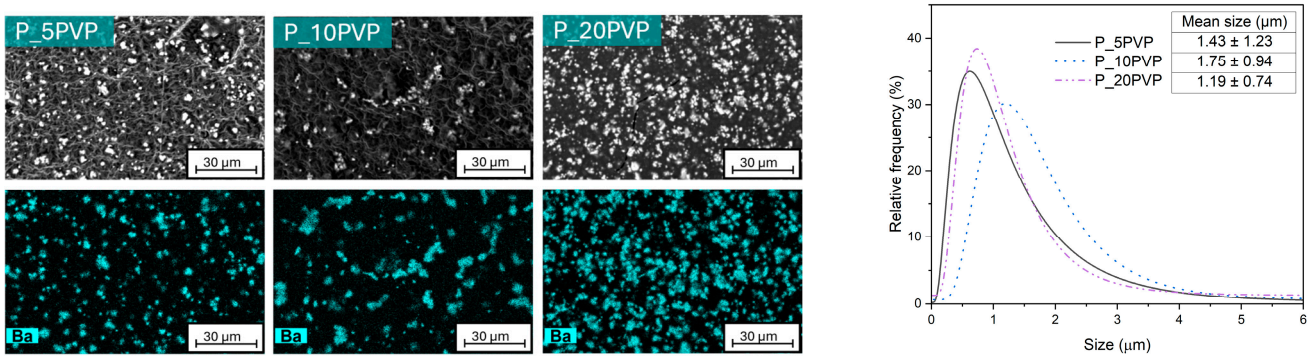

(**a**) (**b**)

Figure 3. (**a**) EDXS barium elemental maps and images of the reference areas of PVDF-TrFE/$BaTiO_3$ composites, prepared using PVP as dispersant, (**b**) relative lognormal size distribution of $BaTiO_3$ within the nanocomposite samples.

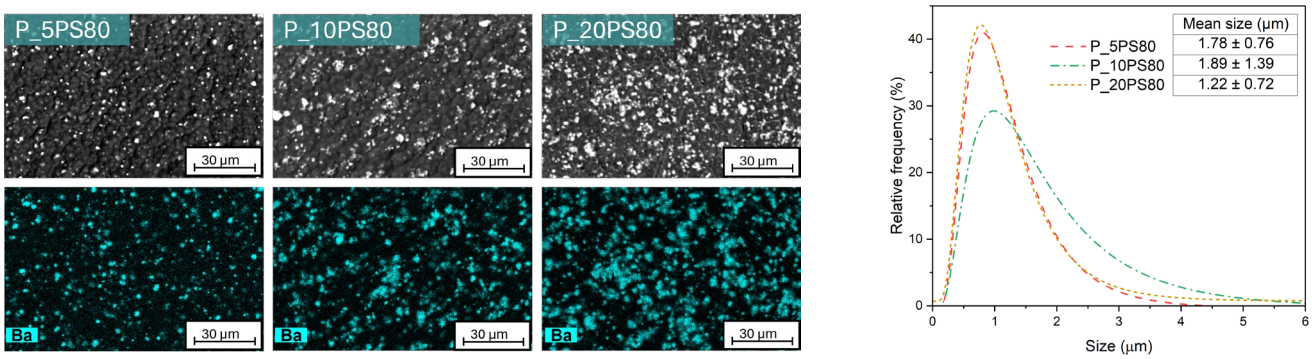

(**a**) (**b**)

Figure 4. (**a**) EDXS barium elemental maps and images of the reference areas of PVDF-TrFE/$BaTiO_3$ composites, prepared using PS80 as dispersant, (**b**) relative lognormal size distribution of $BaTiO_3$ within the nanocomposite samples.

SEM micrographs of the PVDF-TrFE/$BaTiO_3$ composite films are reported in Figure 5. $BaTiO_3$ powder appears as irregularly shaped particles with a broad size distribution. Most grains are in the submicron to ~2–3 µm range, with evident angular morphology and faceted surfaces, typical of crushed or calcined ceramic powders. With reference to the composites, no significant macroscopic defects in the matrix, such as widespread porosity, are observed, indicating that the solvent casting process ensured good film densification and structural integrity, regardless of the dispersant used (PS80 or PVP) and filler loading. The ceramic particles appear in some cases well embedded within the polymer matrix without evident particle pull-out cavities, suggesting adequate interfacial adhesion between $BaTiO_3$ and PVDF-TrFE, even if Figure 5i reports that in some cases the adhesion does not seem adequate. Figure 5i also allows to appreciate the common feature of the β-phase grains of the PVDF-TrFE matrix, made up of rod-like crystallites, tens of nanometers in size [45]. The formation of cavities surrounding particles could also be attributed to the differential shrinkage and debonding deriving from the thermal expansion coefficient

mismatch (approximately 8×10^{-5} K^{-1} for PVDF-TrFE [46,47] and 2×10^{-5} K^{-1} for $BaTiO_3$ [48]). A comparison between the two dispersant systems suggests minor differences. At low filler content (5 vol%), $BaTiO_3$ particles are relatively homogeneously distributed within the matrix, with limited evidence of aggregation, both in PS80 and PVP-containing samples. As the filler loading increases (10 and 20 vol%), the agglomerates become more visible, particularly in the 10 vol% samples and with the PVP dispersant. These aggregates behave like single particles; however, they are typically not surrounded by interfacial gaps, indicating effective wetting of the filler by the polymer despite partial clustering.

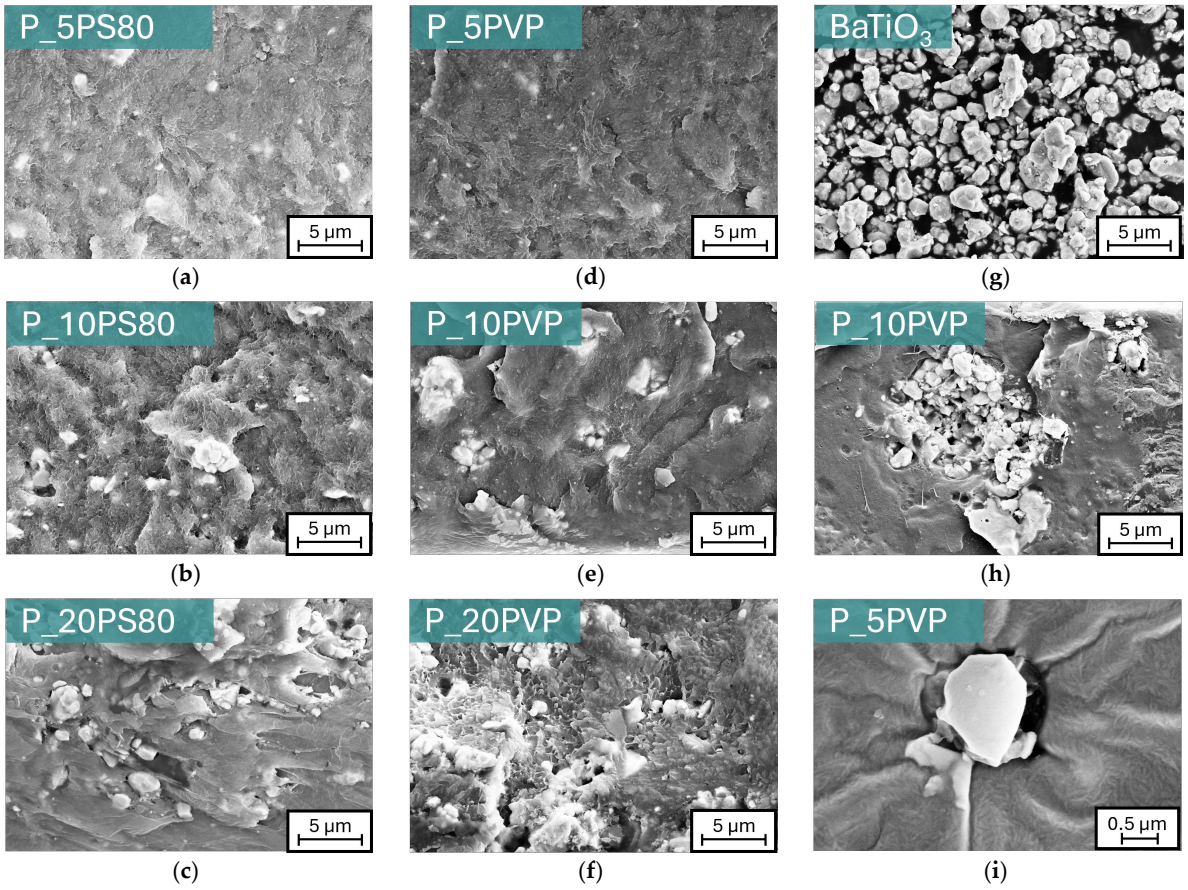

Figure 5. SEM micrographs on the cross-section of the cryofractured surfaces of the nanocomposite films; (**a**–**c**) samples with PS80 at 10 kX magnification, (**d**–**f**) samples with PVP at 10 kX magnification, (**g**) $BaTiO_3$ nanoparticles at 10 kX magnification, (**h**) cluster in a P_10PVP sample at 10 kX magnification, (**i**) single $BaTiO_3$ particle in P_5PVP at 60 kX magnification.

XRD diffractograms and their relative Rietveld analysis are shown in Figure 6, and the main results are reported in Table 2. Figure 6a reports that in all samples, the presence of the β crystalline form of PVDF is immediately confirmed by characteristic Bragg reflections located at 20°, corresponding to the orthorhombic β-phase's (200/110), and at 35° and 41°, corresponding to the planes (001) and (201, 111), respectively [35,49]. Since no diffraction peaks from the α- and γ-phases could be found, the XRD analysis data reveal that the produced samples primarily crystallized in the β-phase. Figure 6c reports how the amorphous region has been simulated with a single Pseudo-Voigt signal with a large FWHM to account for the broad, diffuse shoulder of the main PVDF peak located approximately at 18.5° [23,36], as specified in Section 2.4. In Figure 6a, at 22.2°, 31.5°, 38.9°, and 45.3°, diffraction peaks associated with the perovskite structure of $BaTiO_3$ and belonging, respectively, to the orientation planes (100), (110), (111), and (200) [50] are clearly visible. The Rietveld refinement results (Table 2) indicate a weakly distorted tetragonal structure

of $BaTiO_3$, with a = 3.987–3.992 Å and c = 4.022–4.028 Å, corresponding to a tetragonality factor of c/a = 1.0084–1.0089. These values indicate a stable tetragonal form [37] and are consistent with $BaTiO_3$ particles in the submicrometric regime (~500 nm), where the structure is expected to be bulk-like with minor reduction in lattice distortion due to residual strain or microstructural effects reported in the literature [51]. Upon $BaTiO_3$ incorporation, a significant reduction in the average volume-weighted crystallite size of PVDF-TrFE is observed, decreasing from approximately 236 Å in the neat polymer to values in the range of 120–190 Å in the composites. This reduction indicates a pronounced confinement effect induced by the ceramic filler, which limits crystal growth and promotes the formation of smaller crystalline domains [21]. The addition of $BaTiO_3$ favors the formation of the crystalline fraction of the polymer matrix with a non-monotonic evolution: the reported values are strongly affected by the refinement operation conducted through Rietveld analysis, and should be considered as a qualitative indication of the nucleation effect played by $BaTiO_3$ particles in the PVDF-TrFE systems.

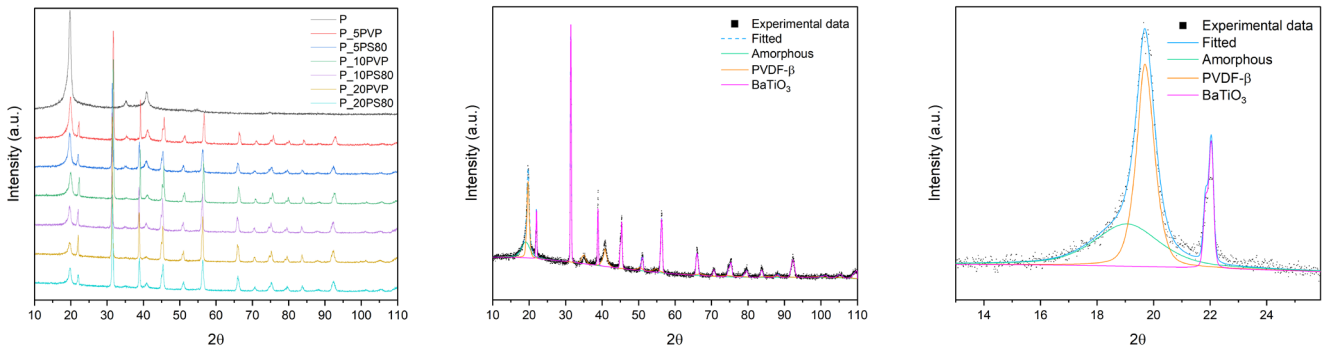

Figure 6. (**a**) XRD diffractograms of all the samples on the whole acquired 2θ range; (**b**) example Rietveld fit as obtained on sample P_5PS80; (**c**) detail of the 13–26° pattern region showing PVDF-β main reflections ((200)/(110)) as well as the signal attributed to the amorphous fraction.

Table 2. Refined parameter values obtained from the Rietveld analysis performed on XRD diffractograms on all the prepared samples.

Sample	PVDF-TrFE		$BaTiO_3$		
	Avg. Domain Size [Å]	Crystalline Fraction [1] (wt%)	a [Å]	c [Å]	c/a
P	236	15.6	N/A	N/A	N/A
P_5PVP	148	21.9	3.99045	4.02409	1.00843
P_10PVP	194	19.0	3.98937	4.02349	1.00855
P_20PVP	190	21.3	3.98911	4.02326	1.00856
P_5PS80	120	20.8	3.99239	4.02772	1.00885
P_10PS80	120	19.6	3.98744	4.02268	1.00884
P_20PS80	134	40.6	3.98757	4.02315	1.00892

[1] Crystalline fraction of the matrix, calculated by normalizing the crystalline percentage of PVDF-TrFE obtained from Rietveld analysis with respect to the weight fraction of the matrix.

Figure 7 reports the FTIR spectra of all the samples in the range 1650 ÷ 550 cm^{-1}. The PVDF-TrFE spectrum shows the three main PVDF bands [52] centered at 880, 1170, and 1400 cm^{-1}, respectively assigned to C-C symmetric vibration, C-C antisymmetric vibration, and CH_2 wagging [53]. The bands at 1072 cm^{-1}, with a barely visible shoulder at 1056 cm^{-1} and at 1119 cm^{-1}, are reported to mark the presence of the TrFE units [52,54], as well as peaks at 1345 cm^{-1} and at 1366 cm^{-1} associated with CHF deformation modes. Resende et al. proposed the origin of these signals from the *tt* and *tg* chain conformation

modes, respectively [54]. Since the presence of the β-phase is the primary determinant of PVDF-TrFE's piezoelectricity, the composites' FTIR spectra were examined to verify the amount of the piezo-active β-phase. The FTIR spectra of neat PVDF-TrFE and its $BaTiO_3$-based composites exhibit an intense absorption band at about 840 cm^{-1}, attributed to the symmetric stretching vibration of the CF_2 groups and commonly regarded as a fingerprint of the electroactive β- and γ-phases [38]. The predominance of the all-trans chain conformation is further corroborated by the presence of characteristic β-phase bands located at 1285 cm^{-1}, 1431 cm^{-1} [54]. A very weak shoulder at approximately 765 cm^{-1}, originating from CF_2 and skeletal bending vibrations related to the TGTG′ chain conformation of the α-phase, can be identified [17,55], as well as CF_3 rocking bands at 975 cm^{-1} [56]. The very low intensity of these features, together with the absence of bands characteristic of the γ-phase (812 cm^{-1}, 832 cm^{-1}, 1245 cm^{-1}), confirms the dominance of the crystalline β-phase in all the prepared PVDF-TrFE/$BaTiO_3$ films. These findings are fully consistent with literature data on PVDF-TrFE copolymers, which are known to preferentially crystallize in the β-phase [54]. The incorporation of $BaTiO_3$ nanoparticles into the PVDF-TrFE matrix does not induce any noticeable band shifts in the FTIR spectra, indicating the absence of specific chemical interactions between the copolymer chains and the ceramic fillers. As reported in Table 3, a very high fraction of the electroactive β-phase is present for neat PVDF-TrFE, reaching approximately 93%, while the nanocomposites show β-phase contents as high as 92%, and never below 90%. These results indicate that the incorporation of $BaTiO_3$ nanoparticles does not hinder the formation of the crystalline β-phase. This observation is in agreement with the literature and confirms that the solvent-based production process predominantly governs the development of the β-phase in both the neat copolymer and the corresponding nanocomposites [23]. The characteristic $BaTiO_3$ absorption bands at ~440 cm^{-1} and ~550 cm^{-1}, which are assigned to the Ti–O stretching and O–Ti–O bending vibrations within the crystal lattice, are not discernible in the composite spectra because they are outside the investigated spectral region, while other $BaTiO_3$ signals are masked by the intense PVDF-TrFE bands occurring in the same spectral regions [37,55].

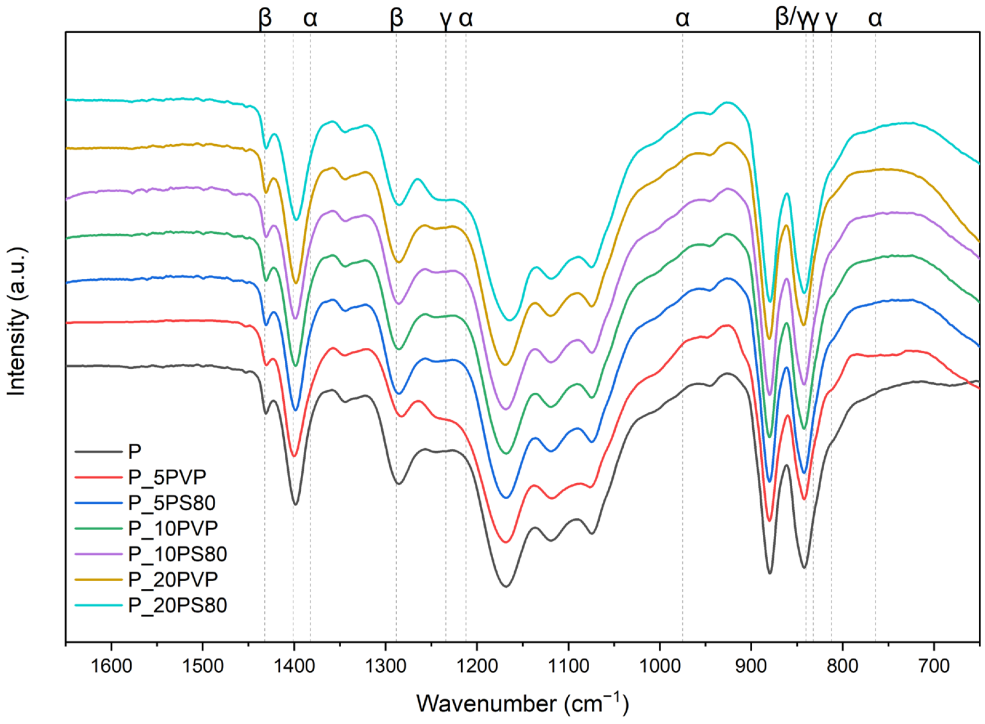

Figure 7. FTIR spectra of the prepared films; the bands related to the different crystalline phases of PVDF are highlighted.

Table 3. Crystalline phases relative amount from FTIR spectra on all the prepared samples.

Sample	F(β,γ) [1] (%)	F(α) [2] (%)
P	93.1	6.9
P_5PVP	89.9	10.1
P_10PVP	92.6	7.4
P_20PVP	92.5	7.5
P_5PS80	90.0	10.0
P_10PS80	92.0	8.0
P_20PS80	91.9	8.1

[1] F(β,γ) = electroactive (β + γ) phase content, determined according to Equation (1); [2] F(α) = 1 − F(β,γ).

DSC thermograms are reported in Figure 8 for PVDF-TrFE and the corresponding $BaTiO_3$-filled composites recorded during the first heating, cooling, and second heating cycles, while the most important numerical results are summarized in Table 4. In all samples, the glass transition temperature is hard to discern in the investigated temperature range. This behavior is attributed to the high degree of crystallinity, which strongly constrains the amorphous fraction and suppresses the signal of T_g, as reported for highly crystalline PVDF-TrFE systems. Moreover, no relaxation phenomena associated with the α-phase are observed, typically reported at 65 °C for neat PVDF [57,58] and in the 40–50 °C range for PVDF copolymers with up to 35 mol.% TrFE unit content [24,57,59]. The absence of such relaxation confirms that the α crystalline fraction is negligible, in agreement with the FTIR results indicating a dominant β-phase content across all compositions. This further supports the conclusion that the adopted production route promotes direct crystallization into the all-trans ferroelectric phase, even in the presence of ceramic fillers. Indeed, achieving a particular sort of crystalline fraction (mainly α, β, γ) depends on whether the crystallization temperature is above or below a specific α nucleation temperature. Gregorio et al. reported the mentioned α onset temperature, for PVDF-TrFE copolymers with 60 and 80 mol% PVDF to be between 70 °C and 80 °C [41,59], which is significantly higher than the 55 °C utilized in this work for the PVDF-TrFE with 75 mol% PVDF. During heating, all samples exhibit a well-defined endothermic peak associated with the ferroelectric to paraelectric transition, related to the Curie temperature (T_c) [21] at 112.6 °C, marginally different from the nominal values suggested by the supplier (116.0 °C). In the composite samples, this ferroelectric-to-paraelectric transition is slightly shifted towards higher temperatures, contrary to what has been reported in the literature for similar systems [21]. At higher temperatures, the melting endothermic peak of the crystalline phase (T_m) at about 150 °C is not significantly influenced by the filler presence. The associated enthalpy (ΔH_m) should be seen in relation to the amount of matrix, revealing the nanoparticles' nucleating effect on the polymer, which leads to an appreciable increase in the total crystallinity of the matrix. This further supports the evidence that both dispersants used in this study have beneficial effects on the filler dispersion. Moreover, the fact that $BaTiO_3$ nanoparticles act as a nucleating agent for the PVDF or PVDF-TrFE is mentioned in the literature only for low filler additions, generally up to 10 vol% [21,23,44], or not reported at all for similar systems [60]. It is possible to correlate the total matrix crystallinity result with the fraction of polar crystalline phase present in the matrix (see Table 3), which remains high even with the addition of $BaTiO_3$. This observation is encouraging, as it demonstrates that increasing the filler volume, even if the effective polymer volume is reduced, preserves the piezoelectric capability of the matrix. Upon cooling, the corresponding exothermic crystallization peaks are clearly visible at around 130 °C for all the samples, while the crystallization enthalpy shows a decreasing trend with the $BaTiO_3$ content. Also, ΔH_{m2} reflects the same trend,

with a peak that stands at around 150 °C for all composites. The paraelectric-to-ferroelectric transition during cooling and the corresponding transition during the second heating stage are clearly visible, thus witnessing the reversible nature of this process. In this instance, the corresponding enthalpies are connected to the energy difference between the paraelectric and the ferroelectric crystalline structures involved in the process [59].

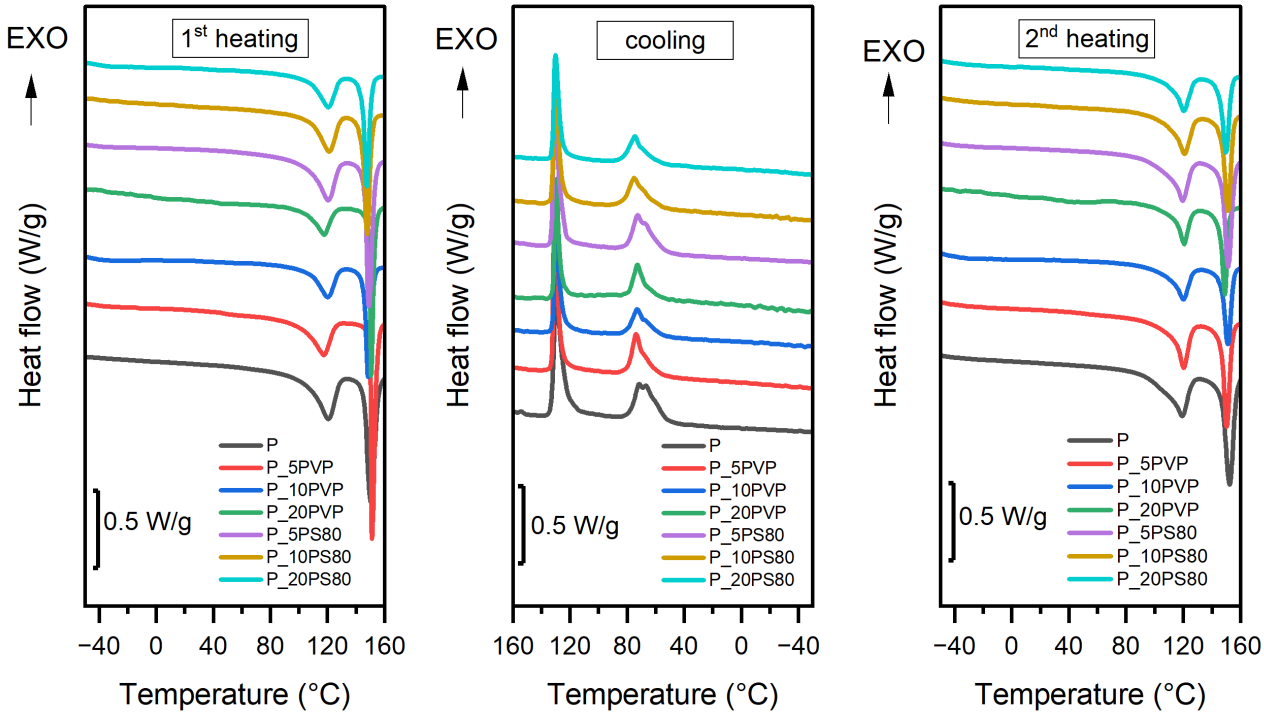

Figure 8. DSC thermograms (first heating, cooling, and second heating scans) of all the samples.

Table 4. Main results of the DSC tests on all the prepared samples.

Sample	T_{m1} (°C)	ΔH_{m1} (J/g)	χ (%)	T_c (°C)	T_{cr} (°C)	ΔH_{cr} (J/g)	T_{m2} (°C)	ΔH_{m2} (J/g)
P	147.9	28.4	27.2	112.6	129.8	30.4	151.7	29.5
P_5PVP	151.3	29.3	32.9	117.3	131.0	25.4	150.4	23.2
P_10PVP	148.6	23.4	31.0	120.0	128.8	22.5	151.4	21.8
P_20PVP	148.6	20.9	35.7	120.2	129.8	20.5	151.2	19.4
P_5PS80	148.0	29.0	32.6	118.1	130.5	26.2	150.9	23.5
P_10PS80	147.8	23.4	31.0	121.4	130.4	24.3	151.1	22.1
P_20PS80	147.5	20.3	34.7	120.2	130.2	18.7	149.9	18.1

T_{m1}, ΔH_{m1} = melting temperature and enthalpy (first heating scan); χ = degree of crystallinity (first heating scan); T_c = Curie temperature (first heating scan); T_{cr}, ΔH_{cr} = crystallization temperature and enthalpy (cooling scan); T_{m2}, ΔH_{m2} = melting temperature and enthalpy (second heating scan).

Thermogravimetric curves are reported in Figure 9, and the main results are summarized in Table 5. PVDF-TrFE shows a first mild degradation until 500 °C and then its characteristic degradation step around 550 °C, with a final residual mass at 700 °C of 11%. On the contrary, $BaTiO_3$ powder, like the majority of inorganic materials, has a very low weight loss of 0.4% and is stable across the whole temperature range. The incorporation of $BaTiO_3$ particles enhances the thermal stability, as evidenced by a shift in the degradation temperature (see Table 5) toward higher temperatures in the presence of the filler, as previously observed for comparable systems [23,60]. The slightly different behavior of composites with PVP compared to those with PS80, visible up to the degradation tempera-

ture, can be attributed to the lower stability of PVP in that temperature range. In fact, it is reported in the literature that PVP, with the molecular weight employed, shows an initial weight loss between 200 °C and 400 °C [61], whereas PS80 remains more stable [62]. After complete decomposition of the polymeric phase, the remaining mass closely matches the nominal $BaTiO_3$ loading without any appreciable difference for systems compatibilized with PVP or PS80, confirming the effective and homogeneous incorporation of the inorganic phase within the composites.

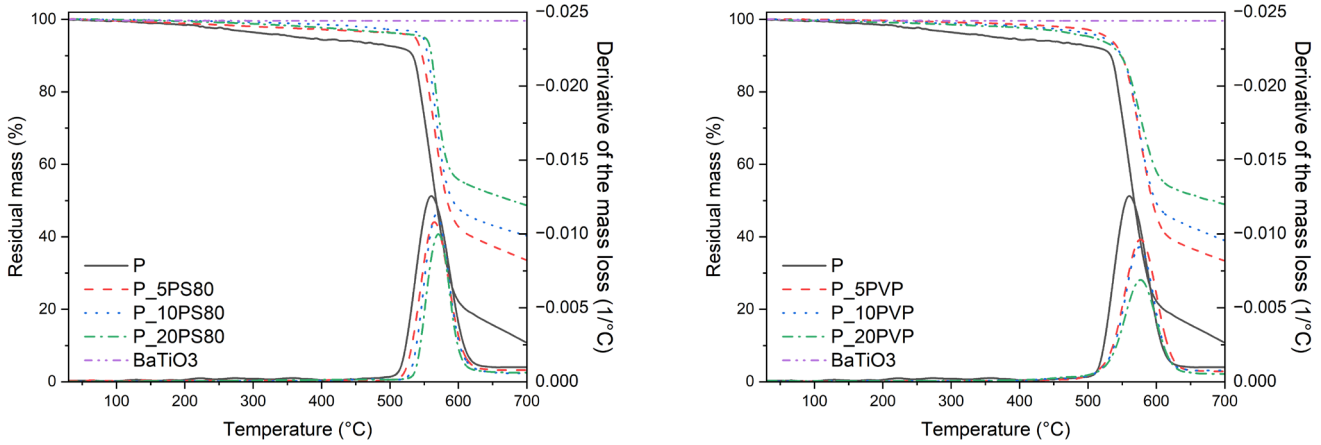

Figure 9. Residual mass and mass loss derivative (DTG) as a function of temperature from TGA tests on samples prepared with (**a**) PS80 dispersant and with (**b**) PVP dispersant.

Table 5. Main results of the TGA tests on the prepared samples.

Sample	$T_{1\%}$ (°C)	$T_{3\%}$ (°C)	$T_{5\%}$ (°C)	T_d (°C)	$m_{r,700}$ (wt%)
P	145.3	271.8	371.2	560.3	10.8
P_5PVP	342.8	503.5	528.9	576.8	33.4
P_10PVP	271.5	470.9	521.5	575.5	39.0
P_20PVP	236.1	445.8	506.5	576.8	49.0
P_5PS80	179.9	427.5	537.1	565.0	33.6
P_10PS80	338.9	516.6	548.6	568.0	40.3
P_20PS80	274.9	451.9	550.5	570.7	48.7
$BaTiO_3$	-	-	-	-	99.6

$T_{1\%}$, $T_{3\%}$, $T_{5\%}$ = temperatures at a mass loss of 1 wt%, 3 wt%, or 5 wt%; T_d = degradation temperature (DTG peak); $m_{r,700}$ = residual mass at 700 °C.

Figure 10 shows the DMTA thermograms (E', E'', and $tan\delta$) of all the samples. As reported in Figure 10a, the storage modulus E' at low temperature grows from approximately 2.1 GPa for neat PVDF-TrFE to about 3.1–3.5 GPa for the 5–10 vol% composites and up to 4.5 GPa for the 20 vol% formulation, indicating the reinforcing effect of the ceramic phase. Moreover, the increase in the storage modulus can be correlated with an increase in the crystallinity of the matrix, as evidenced by data extracted from XRD and DSC. Nonetheless, a progressive decrease of E' with increasing temperature is observed for all samples, confirming that the polymer matrix still governs the viscoelastic response of the composites. From the thermograms of Figure 10b, two main thermal transitions can be recognized. The broad relaxation observed between −35 °C and −20 °C for all samples is probably associated with molecular motions occurring in the amorphous fraction of PVDF-TrFE (glass transition), commonly reported as β or α_a relaxation [63,64]. The increase

in loss modulus at higher temperature is commonly reported for PVDF-based systems as relaxations involving constrained polymer regions (α_c relaxation) and crystal-related motions [65,66] and is associated with a corresponding rise in the damping factor, as visible in Figure 10c. The intensity of this relaxation signal is enhanced with the increasing $BaTiO_3$ mass fraction, particularly for PVP-containing samples, and it is generally shifted towards higher temperatures, indicating a macromolecular constraint effect played by the filler. The maximum tanδ value increases from approximately 0.09 for neat PVDF-TrFE to about 0.12–0.13 for the 20 vol% composites, while the corresponding E″ peaks reach values up to 130 MPa. Overall, the DMTA results demonstrate that the addition of $BaTiO_3$ effectively enhances the stiffness and therefore the dimensional stability of the films, while still retaining good flexibility. This aspect is particularly relevant for flexible piezoelectric and dielectric devices [67].

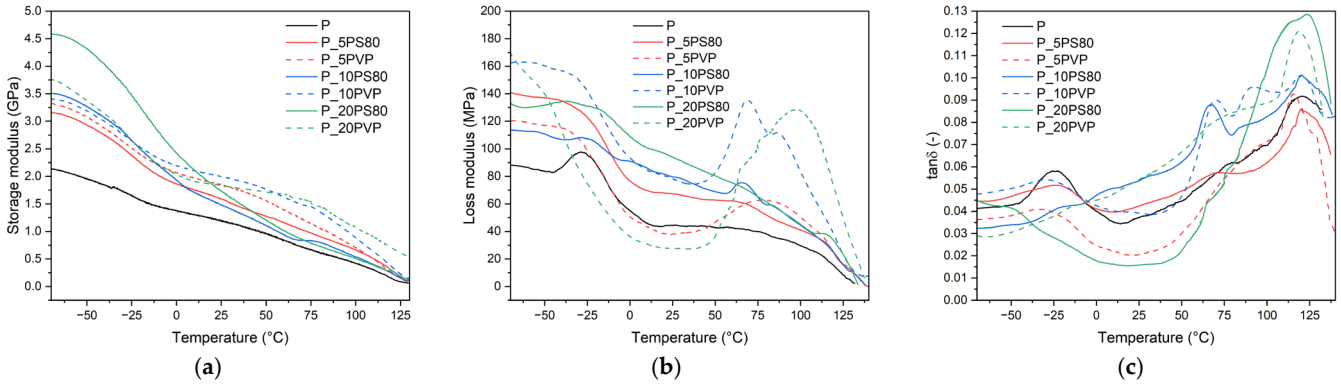

Figure 10. DMTA thermograms of the prepared samples. Trends of (**a**) storage modulus, (**b**) loss modulus, and (**c**) tanδ as a function of the temperature.

The dielectric strength of the PVDF-TrFE/$BaTiO_3$ composites reported in Figure 11a decreases with increasing filler content, as expected from the introduction of a ceramic phase in a polymeric system [68]. In particular, 5 vol% $BaTiO_3$ composites retain a comparatively high dielectric strength, while the 10 and 20 vol% formulations exhibit lower values, yet still remain above a minimum average value of 70 kV/mm (sample P_20PVP), which allows poling at electric fields of a few tens of kV/mm. Overall, it is worth noticing that polysorbate 80 is more effective in preserving a high dielectric strength of the composite. Figure 11b reports the frequency dependence of the relative permittivity (ε_r) at room temperature for PVDF-TrFE/$BaTiO_3$ composites containing different dispersants (PVP and PS80) and filler loading, compared to the neat polymer matrix. Because of the large C–F dipole moment, PVDF and PVDF-based copolymers have the highest dielectric constant among polymeric materials [69]. Neat PVDF-TrFE sample (P) exhibits a nearly frequency-independent permittivity in the investigated range (10^1–10^6 Hz), with $\varepsilon_r \approx 10$–12, characteristic of a stable dipolar polarization of this copolymer with 25%mol of TrFE [70]. The stability of the ε_r values with the frequency confirms the low contribution of space-charge polarization mechanisms in the neat matrix. Upon incorporation of $BaTiO_3$ with PVP as dispersant (P_5PVP, P_10PVP, P_20PVP), ε_r increases moderately and monotonically with the filler content, while preserving a relatively weak frequency dependence. Indeed, real permittivity decreases in all samples passing from low to high frequency regime, and this loss gets more pronounced as the filler fraction rises because of a relaxation mechanism that makes dipolar polarization more difficult at higher frequencies [21,56]. Even at the highest loading (20 vol%), the permittivity decreases only slightly with increasing frequency. This behavior indicates that PVP enables an efficient dispersion of $BaTiO_3$ particles while maintaining electrically stable interfaces. The dielectric response is therefore

mainly governed by intrinsic dipolar polarization of the polymer and the high-permittivity ceramic phase, with a limited contribution from Maxwell–Wagner–Sillars (MWS) interfacial polarization occurring between the matrix and the filler [25,56,60]. In contrast, composites prepared using PS80 dispersant show a markedly different dielectric behavior. At low $BaTiO_3$ contents (P_5PS80 and P_10PS80), ε_r values are comparable to or slightly higher than those of the corresponding PVP-based samples, but a clearer frequency dispersion already emerges, especially below 10^3 Hz. This suggests the onset of interfacial polarization processes associated with the presence of a more mobile, highly polar dispersant at the polymer–filler interface. The effect becomes severe at 20 vol% $BaTiO_3$ (P_20PS80). In this case, ε_r reaches very high values at low frequency (45–50 at 10 Hz) and decreases steeply with the frequency, dropping to 17–18 at 10^5–10^6 Hz. Such a strong dispersion is a clear indication of dominant MWS polarization and space-charge accumulation [71]. At this filler loading, the amount of PS80 (5 wt% relative to $BaTiO_3$) is sufficient to form continuous or quasi-continuous interfacial layers with high dipolar mobility. These soft interphases act as highly polarizable regions at low frequency, but cannot follow the alternating field at higher frequencies, leading to the observed collapse of ε_r. This behavior can be associated with the formation of interfacial regions having dielectric properties different from those of both the ceramic filler and the polymer matrix. Under an alternating electric field, charge carriers and dipoles can accumulate at these heterogeneous interfaces because of the mismatch in conductivity and permittivity between $BaTiO_3$ and PVDF-TrFE, giving rise to MWS interfacial polarization. In composites containing soft organic interphases, the surfactant layer may additionally facilitate local dipolar mobility and charge trapping at the filler/polymer interface, thereby enhancing low-frequency dielectric dispersion and dielectric losses [68]. Figure 11c presents the evolution of the piezoelectric strain coefficient (d_{33}) as a function of the $BaTiO_3$ content. Neat PVDF-TrFE exhibits the highest absolute d_{33} value (−25 pC/N), consistent with the high β-phase content. Upon incorporation of $BaTiO_3$, a gradual decrease in the absolute d_{33} value is observed for both PVP and PS80 nanocomposites, and for both poling routes, with d_{33} approaching −20 pC/N at 20 vol% $BaTiO_3$. This slight decrease in the piezoelectric response suggests that, despite the intrinsic ferroelectricity of $BaTiO_3$, the ceramic nanofiller does not effectively contribute to the macroscopic piezoelectric coefficient of the composite. Recent literature reports d_{33} values for flexible PVDF-TrFE/$BaTiO_3$ composite films typically in the range of 15–35 pC/N for filler contents comparable to those investigated in the present work. In particular, Otero et al. reported d_{33} values of approximately −25 to −33 pC/N for PVDF-TrFE composites containing 10–20 vol% $BaTiO_3$ particles smaller than 500 nm but with higher poling fields [21]. Similar values were also reported for PVDF-TrFE/$BaTiO_3$ nanocomposite mats (−31 pC/N) [24], for PVDF-TrFE/$BaTiO_3$ (7 pC/N), and for $BaTiO_3$/MXene/PVDF-TrFE flexible composites (15.5 pC/N) [72], confirming that the d_{33} values obtained in the present work are consistent with the current state of the art for flexible fluoropolymer-based piezocomposites. In terms of the piezoelectric characteristics, it is crucial to highlight that the generated electric fields in PVDF-TrFE and $BaTiO_3$ have an opposite sign under the same mechanical stress and that their piezoelectric response is thus reversed. As a result, when measured in the same direction as the poling field, the d_{33} values after poling have opposite sign: positive ($d_{33} > 0$) for the ceramic filler and negative ($d_{33} < 0$) for PVDF-TrFE [21,23,24]. Moreover, when a direct current electric field is imposed through a composite material, its allocation among the phases depend on the discharge time (given by the ratio between the permittivity and the conductivity, typical of each phase, according to MWS polarization theory) during a transition period, while it is gradually redistributed depending on the ratio of the resistivities of the constituent phases, in the regime state [73,74]. The observed behavior in the investigated composites can be attributed to the high mismatch in dielectric

permittivity ($\varepsilon_{PVDF\text{-}TrFE} \approx 10$, $\varepsilon_{BaTiO3} \approx 10^3$) and in electric resistivity at the poling temperatures ($\sigma_{PVDF\text{-}TrFE} \approx 10^{11}$ Ω cm [73], $\sigma_{BaTiO3} \approx 10^8$ Ω cm [75]) that result in a rather different electric field distribution among the filler and the matrix [76] both in the transient and in the regime period, that is not sufficient to fully polarize the ceramic phase [77]. Finally, the shifting in the ferroelectric-to-paraelectric transition temperature (see Table 4) results in Curie temperatures of the two phases probably too close to each other, and this has most likely caused the two-step poling to lose its effectiveness. Besides the piezoelectricity, the high dielectric constant obtained can find possible applications in dielectric transducers (actuators and sensors) [78,79] or in systems that combine the functions of a piezoelectric generator and a capacitor within the same material, as proposed by Tong [80].

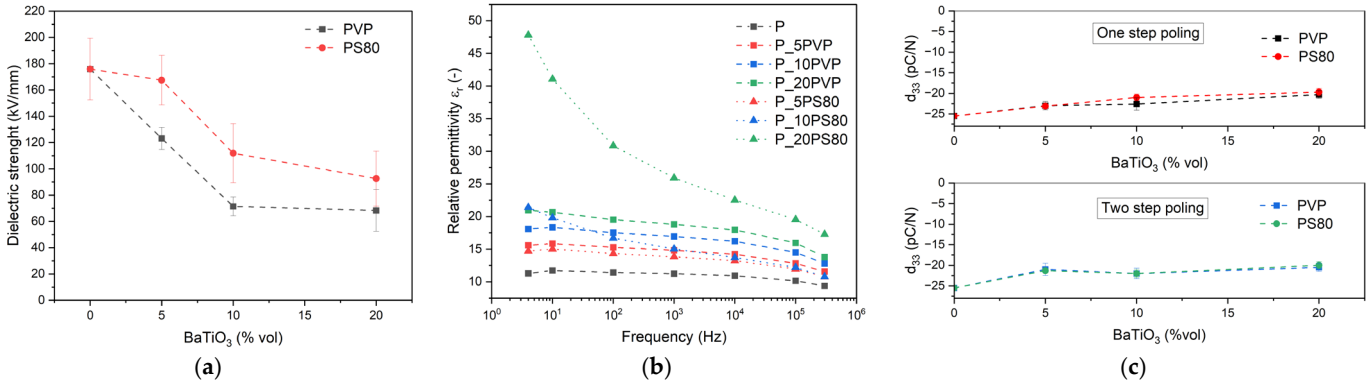

Figure 11. (**a**) Dielectric strength, (**b**) relative permittivity, and (**c**) piezoelectric coefficient (d_{33}) of neat PVDF-TrFE and the relative nanocomposite samples.

4. Conclusions

In this work, PVDF-TrFE/$BaTiO_3$ nanocomposites, prepared using polyvinylpyrrolidone (PVP) or polysorbate 80 (PS80) as dispersants, were successfully fabricated by solvent casting in order to propose a possible route for high dielectric and easy polarizable materials, able to retain high piezoelectric strain coefficient (d_{33}) and possibly synergically exploit the opposite polarity of the matrix and the filler through a carefully designed poling process. The EDXS and SEM comparison between PVP-based and PS80-based systems demonstrated that both dispersants improved filler dispersion, with ceramic nanoparticles firmly embedded in the polymer matrix, indicating good interfacial adhesion between $BaTiO_3$ and PVDF-TrFE. The solvent casting process ensured good film densification and structural integrity, and the crystallization and annealing temperatures allowed the formation and consolidation of the electroactive crystalline β-phase. SEM high-magnification images allowed for distinguishing the rod-like crystallite features of the β-phase in the matrix. FTIR, DSC, and XRD analyses confirmed that the increasing content of $BaTiO_3$ did not influence the relative amount of electroactive phase (which was about 90% of the total matrix crystalline phase) while it favored the nucleation of the crystals in the matrix and moderately influenced the ferroelectric and melting transitions of PVDF-TrFE. DMTA measurements demonstrated that $BaTiO_3$ introduction enhanced the stiffness and the dimensional stability of the samples without substantially compromising their flexibility. Upon incorporation of $BaTiO_3$ through PVP dispersant, ε_r increased moderately and monotonically with filler content, while preserving a relatively weak frequency dependence, indicating that PVP enabled an efficient dispersion of $BaTiO_3$ particles while maintaining electrically stable interfaces. PS80 instead introduced an additional electrically active interfacial phase. At high $BaTiO_3$ volume fractions (20 vol%), the PS80 raised the dielectric response at low frequency and decreased its influence on permittivity with increasing frequency. These results highlighted that, beyond dispersion quality, the electrical

properties of the dispersant play a critical role in controlling interfacial polarization and frequency-dependent dielectric behavior in PVDF-TrFE/$BaTiO_3$ composites. The piezoelectric response was between −20 pC/N and −25 pC/N for all the nanocomposites and was mainly governed by the polymeric phase, while $BaTiO_3$ was poorly poled due to permittivity mismatch and the shift in the matrix Curie temperature toward that of the ceramic, which limits the effectiveness of the two-step poling process on matrix and filler separately. Alternative PVDF-TrFE compositions with different Curie temperatures, or perovskite structures with low permittivity, high d_{33}, and tunable T_c, could address these issues. This type of composite is still not fully explored, and the opposing response of the piezoceramic filler relative to the matrix is often overlooked. Overall, this study evidences the possibility of obtaining high β-phase PVDF copolymer composite films with enhanced dielectric properties while preserving the piezoelectric capabilities of the matrix. Besides piezoelectric applications, the high permittivity achieved by the proposed composites can be used in electrostatic transducer applications.

Author Contributions: Conceptualization, L.B., G.M., S.D. and A.D.; methodology, L.B., G.M., S.D. and A.D.; software, L.B.; validation, L.B.; formal analysis, L.B.; investigation, L.B.; resources, L.B., G.M., S.D. and A.D.; data curation, L.B.; writing—original draft preparation, L.B.; writing—review and editing, G.M., S.D. and A.D.; visualization, L.B.; supervision, G.M., S.D. and A.D.; project administration, L.B. and A.D.; funding acquisition, G.M., S.D. and A.D. All authors have read and agreed to the published version of the manuscript.

Funding: This research was funded by the Department of Excellence 2023–2027 (DE 23–27) program, financed by the Italian Ministry of University and Research (MUR), CUP E63C22003890001.

Data Availability Statement: The raw data supporting the conclusions of this article will be made available by the authors on request.

Acknowledgments: Mauro Bortolotti is gratefully acknowledged for his support in the XRD analysis.

Conflicts of Interest: The authors declare no conflicts of interest. The funders had no role in the design of the study; in the collection, analyses, or interpretation of data; in the writing of the manuscript; or in the decision to publish the results.

Abbreviations

The following abbreviations are used in this manuscript:

$BaTiO_3$	Barium titanate
BoPP	Biaxially oriented polypropylene
DC	Direct current
DMF	N,N-dimethylformamide
PS80	Polysorbate 80
PVDF	Polyvinylidene fluoride
PVDF-TrFE	Poly(vinylidene fluoride-trifluoroethylene)
PVP	Polyvinylpyrrolidone
PZT	Lead zirconate titanate

References

1. Bouhamed, A.; Missaoui, S.; Ben Ayed, A.; Attaoui, A.; Missaoui, D.; Jeder, K.; Guesmi, N.; Njeh, A.; Khemakhem, H.; Kanoun, O. A Comprehensive Review of Strategies toward Efficient Flexible Piezoelectric Polymer Composites Based on $BaTiO_3$ for Next-Generation Energy Harvesting. *Energies* **2024**, *17*, 4066. [CrossRef]
2. Yang, Z.; Zhou, S.; Zu, J.; Inman, D. High-Performance Piezoelectric Energy Harvesters and Their Applications. *Joule* **2018**, *2*, 642–697. [CrossRef]
3. Shu, K.; Li, W.; Wu, Q.; Zong, Y.; Zhao, C.; Zhang, Y.; Wang, C. Polymer-based films for all-in-one piezo-driven self-charging power systems. *J. Mater. Chem. A* **2024**, *12*, 22372–22395. [CrossRef]

4. Zhang, W.; Wu, G.; Zeng, H.; Li, Z.; Wu, W.; Jiang, H.; Zhang, W.; Wu, R.; Huang, Y.; Lei, Z. The Preparation, Structural Design, and Application of Electroactive Poly(vinylidene fluoride)-Based Materials for Wearable Sensors and Human Energy Harvesters. *Polymers* **2023**, *15*, 2766. [CrossRef]
5. Concha, V.O.C.; Timóteo, L.; Duarte, L.A.N.; Bahú, J.O.; Munoz, F.L.; Silva, A.P.; Lodi, L.; Severino, P.; León-Pulido, J.; Souto, E.B. Properties, characterization and biomedical applications of polyvinylidene fluoride (PVDF): A review. *J. Mater. Sci.* **2024**, *59*, 14185–14204. [CrossRef]
6. Wu, L.; Jin, Z.; Liu, Y.; Ning, H.; Liu, X.; Alamusi; Hu, N. Recent advances in the preparation of PVDF-based piezoelectric materials. *Nanotechnol. Rev.* **2022**, *11*, 1386–1407. [CrossRef]
7. Ahbab, N.; Naz, S.; Xu, T.B.; Zhang, S. A Comprehensive Review of Piezoelectric PVDF Polymer Fabrications and Characteristics. *Micromachines* **2025**, *16*, 386. [CrossRef]
8. Li, Y.; Liao, C.; Tjong, S.C. Electrospun Polyvinylidene Fluoride-Based Fibrous Scaffolds with Piezoelectric Characteristics for Bone and Neural Tissue Engineering. *Nanomaterials* **2019**, *9*, 952. [CrossRef]
9. Lovinger, A.J. Annealing of Poly(vinylidene fluoride) and Formation of a Fifth Phase. *Macromolecules* **1982**, *15*, 40–44. [CrossRef]
10. Ruan, L.; Yao, X.; Chang, Y.; Zhou, L.; Qin, G.; Zhang, X. Properties and Applications of the beta Phase Poly(vinylidene fluoride). *Polymers* **2018**, *10*, 228. [CrossRef] [PubMed]
11. Miyashita, T.; Saito, H. Crystal polymorphism of poly(vinylidene fluoride) blended with alkylammonium salts exhibiting different ion-dipole interaction strengths. *Polym. J.* **2023**, *55*, 711–715. [CrossRef]
12. Lovinger, A.J. Ferroelectric polymers. *Science* **1983**, *220*, 1115–1121. [CrossRef] [PubMed]
13. Furukawa, T. Ferroelectric properties of vinylidene fluoride copolymers. *Phase Transit.* **1989**, *18*, 143–211. [CrossRef]
14. Riwa, I.O.; Banyikwa, A.T.; Costa, R.; Veved, A.; Babu, N.S.; Sahini, M.G. Advances in copolymers based on polyvinylidene fluoride (PVDF) and their composites for piezoelectric energy harvesting. *Resour. Chem. Mater.* **2025**, *in press*. [CrossRef]
15. Morali, A.; Mandal, A.; Skorobogatiy, M.; Bodkhe, S. Unleashing the piezoelectric potential of PVDF: A study on phase transformation from gamma (gamma) to beta (beta) phase through thermal contact poling. *RSC Adv.* **2023**, *13*, 31234–31242. [CrossRef]
16. Jia, N.; He, Q.; Sun, J.; Xia, G.; Song, R. Crystallization behavior and electroactive properties of PVDF, P(VDF-TrFE) and their blend films. *Polym. Test.* **2017**, *57*, 302–306. [CrossRef]
17. Meng, N.; Zhu, X.; Mao, R.; Reece, M.J.; Bilotti, E. Nanoscale interfacial electroactivity in PVDF/PVDF-TrFE blended films with enhanced dielectric and ferroelectric properties. *J. Mater. Chem. C* **2017**, *5*, 3296–3305. [CrossRef]
18. Nunes-Pereira, J.; Martins, P.; Cardoso, V.F.; Costa, C.M.; Lanceros-Méndez, S. A green solvent strategy for the development of piezoelectric poly(vinylidene fluoride–trifluoroethylene) films for sensors and actuators applications. *Mater. Des.* **2016**, *104*, 183–189. [CrossRef]
19. Tsyganov, A.; Vikulova, M.; Zotov, I.; Grapenko, O.; Vlasenko, V.; Bainyashev, A.; Gorokhovsky, A.; Gorshkov, N. Thermal behavior of the dielectric response of composites based on poly(vinylidene fluoride) filled with two-dimensional V_2CT_x MXenes. *Nanoscale* **2024**, *16*, 15208–15218. [CrossRef] [PubMed]
20. Sahoo, A.; Paul, T.; Nath, A.; Maiti, S.; Kumar, P.; Ghosh, P.; Banerjee, R. Preferential perovskite surface-termination induced high piezoresponse in lead-free in situ fabricated $Cs_3Bi_2Br_9$-PVDF nanocomposites promotes biomechanical energy harvesting. *Nanoscale* **2023**, *15*, 11603–11615. [CrossRef]
21. Otero, A.; Sayagues, M.J.; Romero, F.J.; Gotor, F.J.; Moriche, R. Piezoelectric and Dielectric Response of $BaTiO_3$/PVDF-TrFE Composites with High beta-Phase Content. *ACS Appl. Polym. Mater.* **2025**, *7*, 7848–7858. [CrossRef]
22. Bodkhe, S.; Turcot, G.; Gosselin, F.P.; Therriault, D. One-Step Solvent Evaporation-Assisted 3D Printing of Piezoelectric PVDF Nanocomposite Structures. *ACS Appl. Mater. Interfaces* **2017**, *9*, 20833–20842. [CrossRef]
23. Kubin, M.; Makreski, P.; Zanoni, M.; Selleri, G.; Gasperini, L.; Fabiani, D.; Gualandi, C.; Bužarovska, A. Piezoelectric properties of PVDF-TrFE/$BaTiO_3$ composite foams with different contents of TrFE units. *Polym. Compos.* **2023**, *44*, 7804–7816. [CrossRef]
24. Stojchevska, E.; Makreski, P.; Zanoni, M.; Gasperini, L.; Selleri, G.; Fabiani, D.; Gualandi, C.; Bužarovska, A. Piezoelectric PVDF-TrFE nanocomposite mats filled with $BaTiO_3$ nanofibers: The effect of poling conditions. *Polym. Adv. Technol.* **2024**, *35*, e6333. [CrossRef]
25. Dang, Z.-M.; Yuan, J.-K.; Zha, J.-W.; Zhou, T.; Li, S.-T.; Hu, G.-H. Fundamentals, processes and applications of high-permittivity polymer–matrix composites. *Prog. Mater. Sci.* **2012**, *57*, 660–723. [CrossRef]
26. Carbone, C.; Benwadih, M.; D'Ambrogio, G.; Le, M.Q.; Capsal, J.F.; Cottinet, P.J. Influence of Matrix and Surfactant on Piezoelectric and Dielectric Properties of Screen-Printed $BaTiO_3$/PVDF Composites. *Polymers* **2021**, *13*, 2166. [CrossRef]
27. Fu, J.; Hou, Y.; Zheng, M.; Wei, Q.; Zhu, M.; Yan, H. Improving Dielectric Properties of PVDF Composites by Employing Surface Modified Strong Polarized $BaTiO_3$ Particles Derived by Molten Salt Method. *ACS Appl. Mater. Interfaces* **2015**, *7*, 24480–24491. [CrossRef] [PubMed]
28. Zamperlin, N.; Bottacini, A.; Callone, E.; Pegoretti, A.; Fontana, M.; Dire, S. Barium Titanate Functionalization with Organosilanes: Effect on Particle Compatibility and Permittivity in Nanocomposites. *Molecules* **2022**, *27*, 6499. [CrossRef]

29. Zamperlin, N.; Sylvestre, A.; Pegoretti, A.; Fontana, M.; Dirè, S. Functionalization of $BaTiO_3$ Nanoparticles to Optimize the Dielectric Performance of Electroactive Polymer Nanocomposites Based on PDMS Matrix. *J. Compos. Sci.* **2026**, *10*, 58. [CrossRef]
30. Kim, Y.-O.; Park, J.J.; Baek, R.; Choi, H.; Jung, D.J.; Lee, J.H. Evaluation of polyvinylpyrrolidone as a dispersant of barium titanate for multilayer ceramic capacitor (MLCC) application. *Macromol. Res.* **2025**, *33*, 895–902. [CrossRef]
31. Kim, T.; Lim, H.; Lee, Y.; Kim, B.J. Synthesis of $BaTiO_3$ nanoparticles as shape modified filler for high dielectric constant ceramic-polymer composite. *RSC Adv.* **2020**, *10*, 29278–29286. [CrossRef] [PubMed]
32. Cortes, H.; Hernandez-Parra, H.; Bernal-Chavez, S.A.; Prado-Audelo, M.L.D.; Caballero-Floran, I.H.; Borbolla-Jimenez, F.V.; Gonzalez-Torres, M.; Magana, J.J.; Leyva-Gomez, G. Non-Ionic Surfactants for Stabilization of Polymeric Nanoparticles for Biomedical Uses. *Materials* **2021**, *14*, 3197. [CrossRef]
33. Ng, W.; Chan, H.L.W.; Choy, C.L. Piezoelectric and Pyroelectric Properties of PZT/P(VDF-TrFE) Composites with Constituent Phases Poled in Parallel or Antiparallel Directions. *IEEE Trans. Ultrason. Ferroelectr. Freq. Control* **2000**, *47*, 1308–1315. [CrossRef] [PubMed]
34. Lutterotti, L. Maud: A Rietveld Analysis Program Designed for the Internet and Experiment Integration. *Acta Crystallogr. Sect. A Found. Crystallogr.* **2000**, *56*, 54. [CrossRef]
35. Hasegawa, R.; Takahashi, Y.; Chatani, Y.; Tadokoro, H. Crystal Structures of Three Crystalline Forms of Poly(vinylidene fluoride). *Polym. J.* **1972**, *3*, 600–610. [CrossRef]
36. Haque, R.I.; Vié, R.; Germainy, M.; Valbin, L.; Benaben, P.; Boddaert, X. Inkjet printing of high molecular weight PVDF-TrFE for flexible electronics. *Flex. Print. Electron.* **2016**, *1*, 015001. [CrossRef]
37. Zamperlin, N.; Ceccato, R.; Fontana, M.; Pegoretti, A.; Chiappini, A.; Dire, S. Effect of Hydrothermal Treatment and Doping on the Microstructural Features of Sol-Gel Derived $BaTiO_3$ Nanoparticles. *Materials* **2021**, *14*, 4345. [CrossRef]
38. Meng, N.; Ren, X.; Santagiuliana, G.; Ventura, L.; Zhang, H.; Wu, J.; Yan, H.; Reece, M.J.; Bilotti, E. Ultrahigh beta-phase content poly(vinylidene fluoride) with relaxor-like ferroelectricity for high energy density capacitors. *Nat. Commun.* **2019**, *10*, 4535. [CrossRef]
39. Elmezayyen, A.S.; Reicha, F.M.; El-Sherbiny, I.M.; Zheng, J.; Xu, C. Significantly enhanced electroactive β phase crystallization and UV-shielding properties in PVDF nanocomposites flexible films through loading of ATO nanoparticles: Synthesis and formation mechanism. *Eur. Polym. J.* **2017**, *90*, 195–208. [CrossRef]
40. Hazarika, D.; Lu, J.; Wu, J.; Shah, M.N.; Li, J.; Zhang, K.; Xu, L.; Chen, C.; Cao, Z.; Jin, H.; et al. Ion dipole interaction and directional alignment enabled high piezoelectric property polyvinylidene fluoride for flexible electronics. *npj Flex. Electron.* **2025**, *9*, 20. [CrossRef]
41. Gregorio, R.J.; Cestari, M. Effect of Crystallization Temperature on the Crystalline Phase Content and Morphology of Poly(vinylidene Fluoride). *J. Polym. Sci. Part B Polym. Phys.* **1994**, *32*, 859–870. [CrossRef]
42. van Krevelen, D.W. *Properties of Polymers: Their Correlation with Chemical Structure; Their Numerical Estimation and Prediction from Additive Group Contributions*, 4th ed.; Elsevier Scientific Pub. Co., Ltd.: Amsterdam, The Netherlands, 2009.
43. Liu, J.; Lu, X.; Wu, C. Effect of Preparation Methods on Crystallization Behavior and Tensile Strength of Poly(vinylidene fluoride) Membranes. *Membranes* **2013**, *3*, 389–405. [CrossRef] [PubMed]
44. Kubin, M.; Makreski, P.; Zanoni, M.; Gasperini, L.; Selleri, G.; Fabiani, D.; Gualandi, C.; Bužarovska, A. Effects of nano-sized $BaTiO_3$ on microstructural, thermal, mechanical and piezoelectric behavior of electrospun PVDF/$BaTiO_3$ nanocomposite mats. *Polym. Test.* **2023**, *126*, 108158. [CrossRef]
45. Hu, X.; You, M.; Yi, N.; Zhang, X.; Xiang, Y. Enhanced Piezoelectric Coefficient of PVDF-TrFE Films via In Situ Polarization. *Front. Energy Res.* **2021**, *9*, 621540. [CrossRef]
46. Ng, W.; Ploss, B.; Chan, H.; Shin, F.; Choy, C. Pyroelectric properties of PZT/P(VDF-TrFE) 0-3 composites. In *ISAF 2000. Proceedings of the 2000 12th IEEE International Symposium on Applications of Ferroelectrics (IEEE Cat. No. 00CH37076)*; IEEE: Honolulu, HI, USA, 2000.
47. Sun, F.-C.; Dongare, A.M.; Asandei, A.D.; Pamir Alpay, S.; Nakhmanson, S. Temperature dependent structural, elastic, and polar properties of ferroelectric polyvinylidene fluoride (PVDF) and trifluoroethylene (TrFE) copolymers. *J. Mater. Chem. C* **2015**, *3*, 8389–8396. [CrossRef]
48. Han, M.; Rong, Y.; Li, Q.; Xing, X.; Kang, L. Thermal expansion of nano-sized $BaTiO_3$. *CrystEngComm* **2015**, *17*, 1944–1951. [CrossRef]
49. Lutkenhaus, J.L.; McEnnis, K.; Serghei, A.; Russell, T.P. Confinement Effects on Crystallization and Curie Transitions of Poly(vinylidene fluoride-co-trifluoroethylene). *Macromolecules* **2010**, *43*, 3844–3850. [CrossRef]
50. Pasuk, I.; Neatu, F.; Neatu, S.; Florea, M.; Istrate, C.M.; Pintilie, I.; Pintilie, L. Structural Details of $BaTiO_3$ Nano-Powders Deduced from the Anisotropic XRD Peak Broadening. *Nanomaterials* **2021**, *11*, 1121. [CrossRef]
51. Zhao, Z.; Buscaglia, V.; Viviani, M.; Buscaglia, M.T.; Mitoseriu, L.; Testino, A.; Nygren, M.; Johnsson, M.; Nanni, P. Grain-size effects on the ferroelectric behavior of dense nanocrystalline $BaTiO_3$ ceramics. *Phys. Rev. B* **2004**, *70*, 024107. [CrossRef]

52. Arrigoni, A.; Brambilla, L.; Bertarelli, C.; Serra, G.; Tommasini, M.; Castiglioni, C. P(VDF-TrFE) nanofibers: Structure of the ferroelectric and paraelectric phases through IR and Raman spectroscopies. *RSC Adv.* **2020**, *10*, 37779–37796. [CrossRef]
53. Cortili, G.; Zerbi, G. Chain conformations of polyvinylidene fluoride as derived from its vibrational spectrum. *Spectrochim. Acta Part A Mol. Spectrosc.* **1967**, *23*, 285–299. [CrossRef]
54. Resende, P.M.; Isasa, J.-D.; Hadziioannou, G.; Fleury, G. Deciphering TrFE Fingerprints in P(VDF-TrFE) by Raman Spectroscopy: Defect Quantification and Morphotropic Phase Boundary. *Macromolecules* **2023**, *56*, 9673–9684. [CrossRef]
55. Hussein, M.M.; Saafan, S.A.; Abosheiasha, H.F.; Kamal, A.A.; Mahmoud, A.E.-r.; Zhou, D.; Trukhanov, S.V.; Zubar, T.I.; Trukhanov, A.V.; Darwish, M.A. Structural and dielectric characterization of synthesized nano-BSTO/PVDF composites for smart sensor applications. *Mater. Adv.* **2023**, *4*, 5605–5617. [CrossRef]
56. Hao, Y.N.; Bi, K.; O'Brien, S.; Wang, X.X.; Lombardi, J.; Pearsall, F.; Li, W.L.; Lei, M.; Wu, Y.; Li, L.T. Interface structure, precursor rheology and dielectric properties of $BaTiO_3$/PVDF–hfp nanocomposite films prepared from colloidal perovskite nanoparticles. *RSC Adv.* **2017**, *7*, 32886–32892. [CrossRef]
57. Teyssèdre, G.; Lacabanne, C. Study of the thermal and dielectric behavior of P(VDF-TrFE) copolymers in relation with their electroactive properties. *Ferroelectrics* **1995**, *171*, 125–144. [CrossRef]
58. Sajkiewicz, P. Crystallization behaviour of poly(vinylidene fluoride). *Eur. Polym. J.* **1999**, *35*, 1581–1590. [CrossRef]
59. Gregorio, R.J.; Botta, M.M. Effect of crystallization temperature on the phase transitions of P(VDF/TrFE) copolymers. *J. Polym. Sci. Part B Polym. Phys.* **1998**, *36*, 403–414. [CrossRef]
60. Mendes, S.F.; Costa, C.M.; Caparros, C.; Sencadas, V.; Lanceros-Méndez, S. Effect of filler size and concentration on the structure and properties of poly(vinylidene fluoride)/$BaTiO_3$ nanocomposites. *J. Mater. Sci.* **2011**, *47*, 1378–1388. [CrossRef]
61. Jablonski, A.E.; Lang, A.J.; Vyazovkin, S. Isoconversional kinetics of degradation of polyvinylpyrrolidone used as a matrix for ammonium nitrate stabilization. *Thermochim. Acta* **2008**, *474*, 78–80. [CrossRef]
62. Kishore, R.S.; Pappenberger, A.; Dauphin, I.B.; Ross, A.; Buergi, B.; Staempfli, A.; Mahler, H.C. Degradation of polysorbates 20 and 80: Studies on thermal autoxidation and hydrolysis. *J. Pharm. Sci.* **2011**, *100*, 721–731. [CrossRef]
63. Mano, J.F.; Sencadas, V.; Costa, A.M.; Lanceros-Méndez, S. Dynamic mechanical analysis and creep behaviour of β-PVDF films. *Mater. Sci. Eng. A* **2004**, *370*, 336–340. [CrossRef]
64. Liu, Z.; Maréchal, P.; Jérôme, R. D.m.a. and d.s.c, investigations of the β transition of poly(vinylidene fluoride). *Polymer* **1997**, *38*, 4925–4929. [CrossRef]
65. Sencadas, V.; Lanceros-Mendez, S.; Sabater i Serra, R.; Andrio Balado, A.; Gomez Ribelles, J.L. Relaxation dynamics of poly(vinylidene fluoride) studied by dynamical mechanical measurements and dielectric spectroscopy. *Eur. Phys. J. E Soft Matter* **2012**, *35*, 41. [CrossRef] [PubMed]
66. Sy, J.W.; Mijovic, J. Reorientational Dynamics of Poly(vinylidene fluoride)/Poly(methyl methacrylate) Blends by Broad-Band Dielectric Relaxation Spectroscopy. *Macromolecules* **2000**, *33*, 933–946. [CrossRef]
67. Taleb, S.; Badillo, M.; Flores-Ruiz, F.J.; Acuautla, M. From synthesis to application: High-quality flexible piezoelectric sensors fabricated from tetragonal $BaTiO_3$/P(VDF-TrFE) composites. *Sens. Actuators A Phys.* **2023**, *361*, 114585. [CrossRef]
68. Hou, Y.; Deng, Y.; Wang, Y.; Gao, H. Uniform distribution of low content $BaTiO_3$ nanoparticles in poly(vinylidene fluoride) nanocomposite: Toward high dielectric breakdown strength and energy storage density. *RSC Adv.* **2015**, *5*, 72090–72098. [CrossRef]
69. Soulestin, T.; Ladmiral, V.; Dos Santos, F.D.; Améduri, B. Vinylidene fluoride- and trifluoroethylene-containing fluorinated electroactive copolymers. How does chemistry impact properties? *Prog. Polym. Sci.* **2017**, *72*, 16–60. [CrossRef]
70. Yagi, T.; Tatemoto, M.; Sako, J.-i. Transition Behavior and Dielectric Properties in Trifluoroethylene and Vinylidene Fluoride Copolymers. *Polym. J.* **1980**, *12*, 209–223. [CrossRef]
71. Jian, G.; Jiao, Y.; Meng, Q.; Wei, Z.; Zhang, J.; Yan, C.; Moon, K.-S.; Wong, C.-P. Enhanced dielectric constant and energy density in a $BaTiO_3$/polymer-matrix composite sponge. *Commun. Mater.* **2020**, *1*, 91. [CrossRef]
72. Liu, X.; Tong, J.; Wang, J.; Lu, S.; Yang, D.; Li, H.; Liua, C.; Song, Y. $BaTiO_3$/MXene/PVDF-TrFE composite films via an electrospinning method for flexible piezoelectric pressure sensors. *J. Mater. Chem. C* **2023**, *11*, 4614–4622. [CrossRef]
73. Selleri, G.; Gino, M.E.; Brugo, T.M.; D'Anniballe, R.; Tabucol, J.; Focarete, M.L.; Carloni, R.; Fabiani, D.; Zucchelli, A. Self-sensing composite material based on piezoelectric nanofibers. *Mater. Des.* **2022**, *219*, 110787. [CrossRef]
74. Sîrbu, I.-D.; Preninger, D.; Danninger, D.; Penkner, L.; Schwödiauer, R.; Moretti, G.; Arnold, N.; Fontana, M.; Kaltenbrunner, M. Electrostatic actuators with constant force at low power loss using matched dielectrics. *Nat. Electron.* **2023**, *6*, 888–899. [CrossRef]
75. Sareecha, N.; Ali Shah, W.; Anis-ur-Rehman, M.; Latif Mirza, M.; Awan, M.S. Electrical investigations of $BaTiO_3$ ceramics with Ba/Ti contents under influence of temperature. *Solid State Ion.* **2017**, *303*, 16–23. [CrossRef]
76. Padurariu, L.; Brunengo, E.; Canu, G.; Curecheriu, L.P.; Conzatti, L.; Buscaglia, M.T.; Stagnaro, P.; Mitoseriu, L.; Buscaglia, V. Role of Microstructures in the Dielectric Properties of PVDF-Based Nanocomposites Containing High-Permittivity Fillers for Energy Storage. *ACS Appl. Mater. Interfaces* **2023**, *15*, 13535–13544. [CrossRef]

77. Belovickis, J.; Ivanov, M.; Svirskas, Š.; Samulionis, V.; Banys, J.; Solnyshkin, A.V.; Gavrilov, S.A.; Nekludov, K.N.; Shvartsman, V.V.; Silibin, M.V. Dielectric, Ferroelectric, and Piezoelectric Investigation of Polymer-Based P(VDF-TrFE) Composites. *Phys. Status Solidi (B)* **2017**, *255*, 1700196. [CrossRef]
78. Gravert, S.-D.; Varini, E.; Kazemipour, A.; Michelis, M.Y.; Buchner, T.; Hinchet, R.; Katzschmann, R.K. Low-voltage electrohydraulic actuators foruntethered robotics. *Sci. Adv.* **2024**, *10*, eadi9319. [CrossRef]
79. Wang, S.; Yang, C.; Li, X.; Jia, H.; Liu, S.; Liu, X.; Minari, T.; Sun, Q. Polymer-based dielectrics with high permittivity and low dielectric loss for flexible electronics. *J. Mater. Chem. C* **2022**, *10*, 6196–6221. [CrossRef]
80. Tong, W.; Zhang, Y.; Zhang, Q.; Luan, X.; Lv, F.; Liu, L.; An, Q. An All-Solid-State Flexible Piezoelectric High-k Film Functioning as Both a Generator and In Situ Storage Unit. *Adv. Funct. Mater.* **2015**, *25*, 7029–7037. [CrossRef]

Disclaimer/Publisher's Note: The statements, opinions and data contained in all publications are solely those of the individual author(s) and contributor(s) and not of MDPI and/or the editor(s). MDPI and/or the editor(s) disclaim responsibility for any injury to people or property resulting from any ideas, methods, instructions or products referred to in the content.